Article

Cell Chemical Biology

Increased energy demand from anabolic-catabolic processes drives β-lactam antibiotic lethality

Graphical abstract

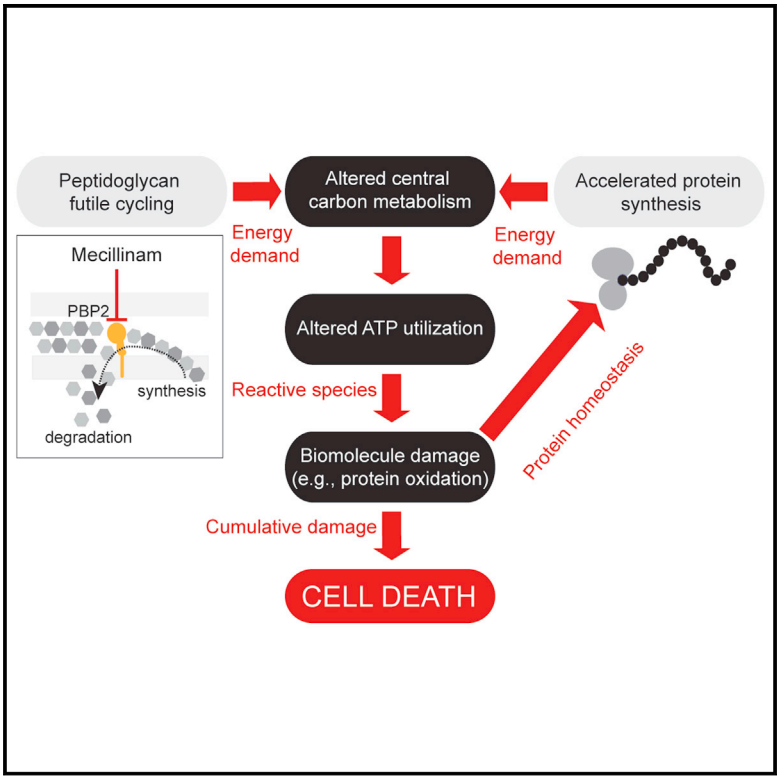

Highlights

- PBP2 inhibition by mecillinam alters bacterial catabolic and anabolic processes
- Bacterial protein synthesis is identified as a source of energy demand
- Reactive metabolic by-products are important for mecillinam lethality
- Target-proximal and downstream metabolic effects contribute to mecillinam lethality

Authors

Michael A. Lobritz, Ian W. Andrews, Dana Braff, ..., Graham C. Walker, Daniel J. Dwyer, James J. Collins

Correspondence

djdwyer@umd.edu (D.J.D.), jimjc@mit.edu (J.J.C.)

In brief

Lobritz et al. assess the target-proximal and downstream metabolic consequences of treatment of *E. coli* with the β-lactam mecillinam. They show that lethality from PBP2 inhibition is a specific consequence of toxic metabolic shifts induced by energy demand from multiple catabolic and anabolic processes.

Lobritz et al., 2022, Cell Chemical Biology *29*, 1–11
February 17, 2022
https://doi.org/10.1016/j.chembiol.2021.12.010

CellPress

Please cite this article in press as: Lobritz et al., Increased energy demand from anabolic-catabolic processes drives β-lactam antibiotic lethality, Cell Chemical Biology (2021), https://doi.org/10.1016/j.chembiol.2021.12.010

Cell Chemical Biology

CellPress
OPEN ACCESS

Article

Increased energy demand from anabolic-catabolic processes drives β-lactam antibiotic lethality

Michael A. Lobritz,[1,2,3,4,10,14] Ian W. Andrews,[1,2,3,14] Dana Braff,[1,2,5,11] Caroline B.M. Porter,[2,3] Arnaud Gutierrez,[2,3,12] Yoshikazu Furuta,[2,13] Louis B.G. Cortes,[6] Thomas Ferrante,[1] Sarah C. Bening,[2,3] Felix Wong,[2,3] Charley Gruber,[7] Christopher W. Bakerlee,[2,3] Guillaume Lambert,[6] Graham C. Walker,[7] Daniel J. Dwyer,[8,*] and James J. Collins[1,2,3,9,15,*]

[1]Wyss Institute for Biologically Inspired Engineering, Harvard University, Boston, MA 02115, USA
[2]Institute for Medical Engineering & Science, Department of Biological Engineering, and Synthetic Biology Center, Massachusetts Institute of Technology, Cambridge, MA 02139, USA
[3]Broad Institute of MIT and Harvard, Cambridge, MA 02139, USA
[4]Division of Infectious Diseases, Massachusetts General Hospital, Boston, MA 02114, USA
[5]Department of Biomedical Engineering, Boston University, Boston, MA 02215, USA
[6]School of Applied and Engineering Physics, Cornell University, Ithaca, NY 14853, USA
[7]Department of Biology, Massachusetts Institute of Technology, Cambridge, MA 02139, USA
[8]Department of Cell Biology and Molecular Genetics, Institute for Physical Science and Technology, Department of Biomedical Engineering, and Maryland Pathogen Research Institute, University of Maryland, College Park, MD 20742, USA
[9]Harvard-MIT Program in Health Sciences and Technology, Cambridge, MA 02139, USA
[10]Present address: Roche Pharma Research and Early Development, Roche Innovation Center Basel, 4070 Basel, Switzerland
[11]Present address: GRO Biosciences, Cambridge, MA 02139, USA
[12]Present address: Institut Cochin, INSERM U1016 – CNRS UMR8104 – Université Paris Descartes, 75014 Paris, France
[13]Present address: Research Center for Zoonosis Control, Hokkaido University, Sapporo 001-0020, Japan
[14]These authors contributed equally
[15]Lead contact
*Correspondence: djdwyer@umd.edu (D.J.D.), jimjc@mit.edu (J.J.C.)
https://doi.org/10.1016/j.chembiol.2021.12.010

SUMMARY

β-Lactam antibiotics disrupt the assembly of peptidoglycan (PG) within the bacterial cell wall by inhibiting the enzymatic activity of penicillin-binding proteins (PBPs). It was recently shown that β-lactam treatment initializes a futile cycle of PG synthesis and degradation, highlighting major gaps in our understanding of the lethal effects of PBP inhibition by β-lactam antibiotics. Here, we assess the downstream metabolic consequences of treatment of *Escherichia coli* with the β-lactam mecillinam and show that lethality from PBP2 inhibition is a specific consequence of toxic metabolic shifts induced by energy demand from multiple catabolic and anabolic processes, including accelerated protein synthesis downstream of PG futile cycling. Resource allocation into these processes is coincident with alterations in ATP synthesis and utilization, as well as a broadly dysregulated cellular redox environment. These results indicate that the disruption of normal anabolic-catabolic homeostasis by PBP inhibition is an essential factor for β-lactam antibiotic lethality.

INTRODUCTION

β-Lactam antibiotics are the preferred first line of therapy for the treatment of a broad range of bacterial infections. From a drug-target perspective, it is well understood that β-lactam antibiotics bind to and irreversibly inactivate a suite of enzymes, referred to as penicillin-binding proteins (PBPs), which play a critical role in peptidoglycan (PG) biosynthesis within the bacterial cell wall (Spratt and Cromie, 1988). The precise description of how PBP inhibition by β-lactam antibiotics leads to cell death is confounded, however, by the fact that many β-lactams simultaneously inhibit multiple PBP proteins that function in distinct, growth-phase-dependent steps in bacterial cell elongation and division (Spratt, 1975; Typas et al., 2011). While inhibition of bifunctional class A PBPs, possessing both transpeptidase and glycosyltransferase activity, results in rapid cell lysis (Yousif et al., 1985), inhibition of monofunctional class B PBPs (PBP2 or PBP3) with only transpeptidase activity yields morphologically distinct outcomes and ultimately bacterial cell death (Spratt, 1975). This understanding of PBP activity has been enhanced by recent findings revealing that there are SEDS (shape, elongation, division, sporulation)-family proteins with glycosyltransferase activity that perform PG biogenesis in complex with class B PBPs (Cho et al., 2016; Egan et al., 2020; Meeske et al., 2016).

Investigating the complexity of bacterial responses to PBP inhibition has been made tractable by the use of chemical biology approaches that target single PBPs. For example, inhibition of PBP2 in rod-shaped bacteria by the specific inhibitor mecillinam,

Please cite this article in press as: Lobritz et al., Increased energy demand from anabolic-catabolic processes drives β-lactam antibiotic lethality, Cell Chemical Biology (2021), https://doi.org/10.1016/j.chembiol.2021.12.010

commonly prescribed to treat urinary tract infections caused by susceptible Gram-negative pathogens, disrupts the Gram-negative bacterial Rod system resulting in spheroplast formation and cell death (Spratt, 1975). It has since been shown in a PG recycling mutant that PBP2 target inhibition by mecillinam leads to degradation of new PG polymers, while PG biosynthesis itself is unaffected (Uehara and Park, 2008). Subsequent work involving mapping of the fate of PG precursors expanded this finding to reveal that PBP2 inhibition initializes a futile cycle of PG synthesis and degradation (Cho et al., 2014). Interruption of this futile cycle by chemical or genetic means was shown to uncouple PBP2 inhibition from lethality, suggesting that the impact of unsynchronized PG turnover is a key contributor to bactericidal activity. Additionally, these findings expand our understanding of the decades-old observation that the lethality of lysis-triggering β-lactams can be preserved even when lysis is genetically inhibited (Moreillon et al., 1990).

Recent work in *Mycobacterium bovis* has revealed that cell wall synthesis inhibitors (including the nonspecific PBP2 inhibiting β-lactam, meropenem) stimulate an increase in ATP production (Shetty and Dick, 2018). In a follow-on study, it was shown in *Mycobacterium abscessus* that suppressing this increased ATP production with the ATP synthase inhibitor bedaquiline eliminated the lethal effects of β-lactams (Lindman and Dick, 2019). Recent work examining L-form growth in Gram-positive bacteria linked the toxicity of β-lactam treatment to an increase in glycolytic flux resulting in the production of toxic reactive oxygen species by the respiratory chain (Kawai et al., 2019). These results are consistent with previous observations regarding toxic changes in tricarboxylic acid (TCA) cycle activity and respiratory behaviors in *Escherichia coli* challenged with β-lactams (Belenky et al., 2015; Dwyer et al., 2014; Foti et al., 2012; Kohanski et al., 2007), all of which accompany activation of canonical SOS general stress (Miller et al., 2004) and envelope stress responses (Delhaye et al., 2016; Guest and Raivio, 2016; Kohanski et al., 2008; Laubacher and Ades, 2008). Despite these associations, the mechanistic connections between upstream target-proximal perturbations of β-lactam treatment and downstream metabolic processes remain poorly understood.

Here, we exploit the target specificity of mecillinam to test the hypothesis that PBP2 inhibition drives changes in cellular metabolism and energy demand that contribute to the lethality of β-lactam antibiotics. Our metabolomics-focused approach reveals that mecillinam treatment results in broad metabolic shifts, altering the activity of central carbon oxidation pathways, amino acid and nucleobase metabolism, and ATP utilization, ultimately leading to a dysregulated cellular redox environment. Our results support and extend the previously identified role for target-proximal PG futile cycling in mecillinam lethality by identifying bacterial protein synthesis as an additional source of energy demand that links PBP inhibition to cellular lethality. Building on these observations, we show that the availability of exogenous amino acids and the presence of reactive metabolic by-products are important factors for mecillinam lethality. Together, these data link the target-proximal effects of β-lactam antibiotics and downstream cellular metabolic effects, demonstrating that drug-induced disruption of normal anabolic-catabolic homeostasis is an important factor for β-lactam antibiotic activity.

RESULTS

PBP2 inhibition results in broad metabolic shifts in *E. coli*

Inhibition of *E. coli* PBP2 by the β-lactam antibiotic mecillinam has been shown to induce malfunctioning of the bacterial cell wall synthesis machinery, including the formation of a futile cycle of PG synthesis and degradation (Cho et al., 2014). We sought to characterize the bioenergetic consequences of this phenomenon by using a metabolomics approach. For both intracellular and extracellular metabolite measurements, bacteria were grown in M9 minimal medium supplemented with 10 mM glucose as the sole carbon source (M9G). We reasoned that this approach would improve our ability to assess metabolite changes in response to mecillinam treatment. Specifically, mecillinam challenge is rapidly bactericidal for *E. coli* in rich media (Figure 1A), which may confound the attribution of metabolite changes specifically to enzymatic inhibition of PBP2 relative to those that may be a nonspecific component of bacterial cell death. In contrast, mecillinam treatment of *E. coli* in M9G results in a bacteriostatic effect (Joseleau-Petit et al., 1994) (Figure 1A), reducing the contribution of cell death in the measurement of changes in metabolite levels. *E. coli* grown in M9G was treated with a high concentration of mecillinam (10 μg/mL, or 33-fold over the minimum inhibitory concentration), resulting in uniform shape distortion within the bacterial population consistent with inactivation of the Rod system, and suggesting that growth in M9G does not interfere with mecillinam drug-target engagement (Figure 1B). Additionally, we observed that the morphological changes in M9G are more homogeneous and of a smaller magnitude relative to rich media conditions (Figure 1B), an advantage for population-level metabolite comparisons.

To further explore this conditional bacteriostatic phenomenon, we measured extracellular glucose consumption by *E. coli* in response to mecillinam compared with a growth control in M9G. We further compared this with the effect on glucose consumption caused by the translation inhibitor chloramphenicol, an antibiotic that induces bacteriostasis independent of media context. We found that mecillinam treatment increased glucose consumption rate relative to untreated cells (Figure 1C). In contrast, chloramphenicol treatment substantially reduced glucose consumption (Figure 1C). Consistent with this finding for chloramphenicol, previous data have shown a marked decrease in bacterial aerobic metabolism in response to this drug (Lobritz et al., 2015). These results indicate that the bacteriostasis induced in M9G by PBP2 inhibition is associated with distinctly different metabolic responses from the bacteriostasis induced in M9G by translation inhibition.

Since mecillinam treatment increased glucose consumption in M9G, we hypothesized that mecillinam treatment may also be associated with broader changes in the intracellular metabolome. To assess this, we performed targeted, quantitative intracellular metabolomic profiling of *E. coli* by comparing a time course of mecillinam-treated relative to untreated cells grown in M9G batch culture. Samples were taken prior to treatment and then hourly for 4 h, and subjected to capillary electrophoresis-tandem mass spectrometry measurements to obtain absolute quantification measurements for a total of 96 intracellular metabolites and relative quantification of a larger breadth of

Please cite this article in press as: Lobritz et al., Increased energy demand from anabolic-catabolic processes drives β-lactam antibiotic lethality, Cell Chemical Biology (2021), https://doi.org/10.1016/j.chembiol.2021.12.010

CellPress
OPEN ACCESS

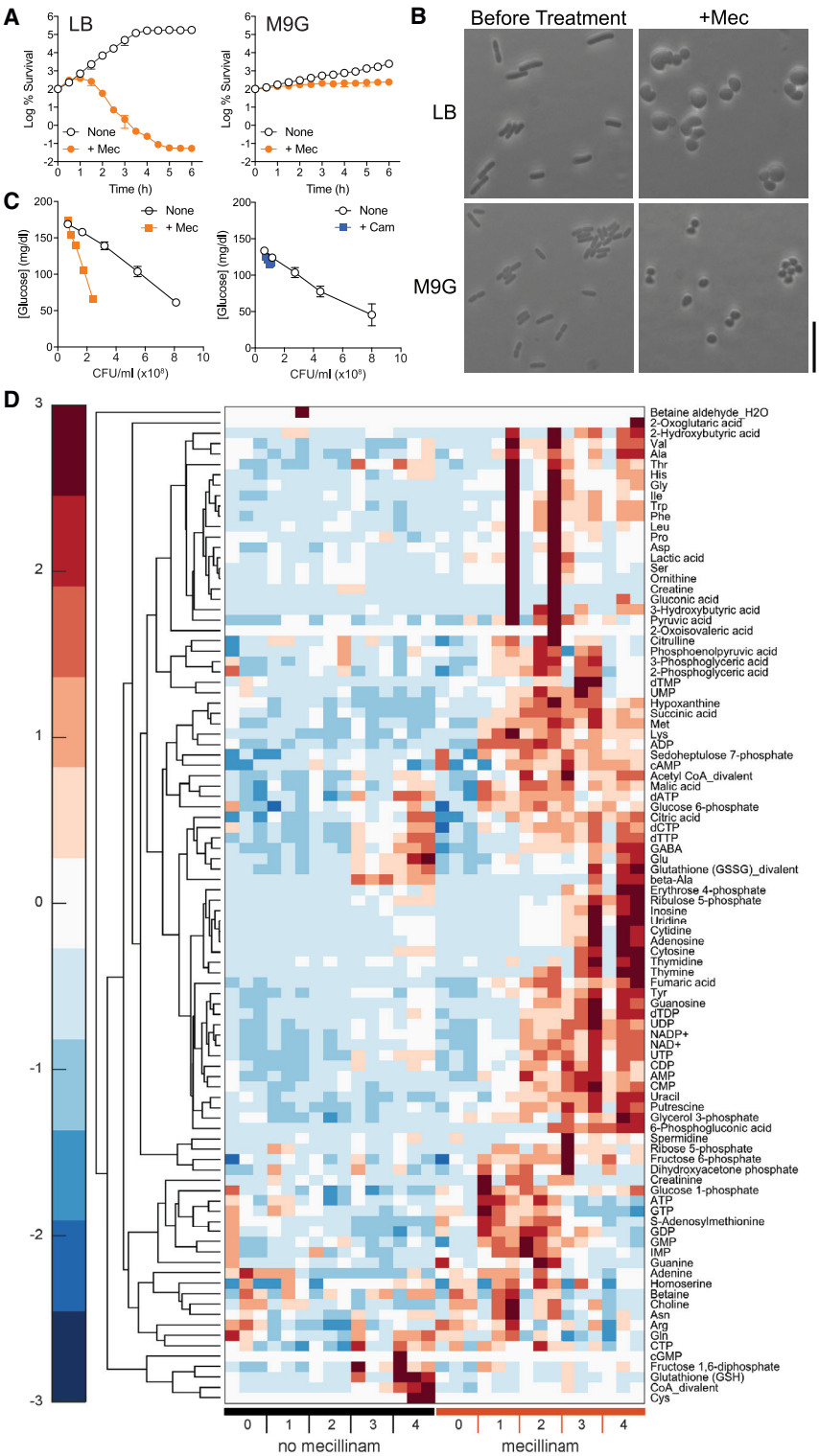

Figure 1. PBP2 inhibition results in broad metabolic shifts in *E. coli*

(A) Time-kill kinetics of mecillinam (Mec, 10 μg/mL) treatment of wild-type *E. coli* MG1655 in LB and M9 medium supplemented with 10 mM glucose as the sole carbon source (M9G). Shown is the mean of three biological replicates. Error bars denote SEM.

(B) Microscopy images of *E. coli* MG1655 grown in LB and M9G, before and after 3 h of treatment with Mec. Scale bar, 10 μm.

(C) Extracellular glucose concentration is plotted relative to corresponding colony-forming units (CFU) under bacteriostatic conditions induced by Mec (left) and chloramphenicol (Cam, 50 μg/mL) (right) from simultaneous cultures taken for intracellular metabolite profiling, grown in M9G. Shown are the means of three biological replicates for Mec and two biological replicates for Cam, respectively. Error bars denote SEM.

(D) Hierarchical clustering of quantified metabolites measured hourly for 4 h using capillary electrophoresis-tandem mass spectrometry for untreated and Mec-treated *E. coli* MG1655 grown in M9G.

See also Figure S1 and Table S1.

metabolites (Figures S1A and S1B; Table S1). Hierarchical clustering and principal component analysis of the metabolites with absolute quantification measurements revealed extensive mecillinam-induced remodeling of the *E. coli* metabolome, including perturbations across central carbon, energy carrier, nucleotide, and amino acid metabolism (Figures 1D and S1C). In the following sections, we further explore this metabolomics dataset and combine it with additional experiments that provide insights into the impact of PBP2 inhibition on the bacterial metabolic state.

PBP2 inhibition alters activity of central carbon pathways and ATP utilization

Within the metabolomics dataset, evaluation of central carbon oxidation pathways revealed that mecillinam treatment in M9G resulted over time in increased quantities of intracellular carbon metabolites within glycolysis and the TCA cycle (Figure 2A), pathways involved in multiple cellular processes including energy generation. Mecillinam treatment further increased the quantities of intracellular metabolites in the anabolic pentose phosphate pathway (Figure 2A), which is critical for the formation of precursor metabolites of amino acid and nucleotide biosynthesis as well as for the formation of NADPH, which is required for glutathione recycling under oxidative stress conditions (Christodoulou et al., 2018).

We hypothesized that toxic malfunctioning of the cell wall synthesis machinery impacts intracellular ATP utilization; this hypothesis was motivated in part by our observation of altered glucose consumption and central carbon oxidation in response to mecillinam treatment. The use of capillary electrophoresis as a metabolomics approach facilitates the measurement of high-energy phosphate

Please cite this article in press as: Lobritz et al., Increased energy demand from anabolic-catabolic processes drives β-lactam antibiotic lethality, Cell Chemical Biology (2021), https://doi.org/10.1016/j.chembiol.2021.12.010

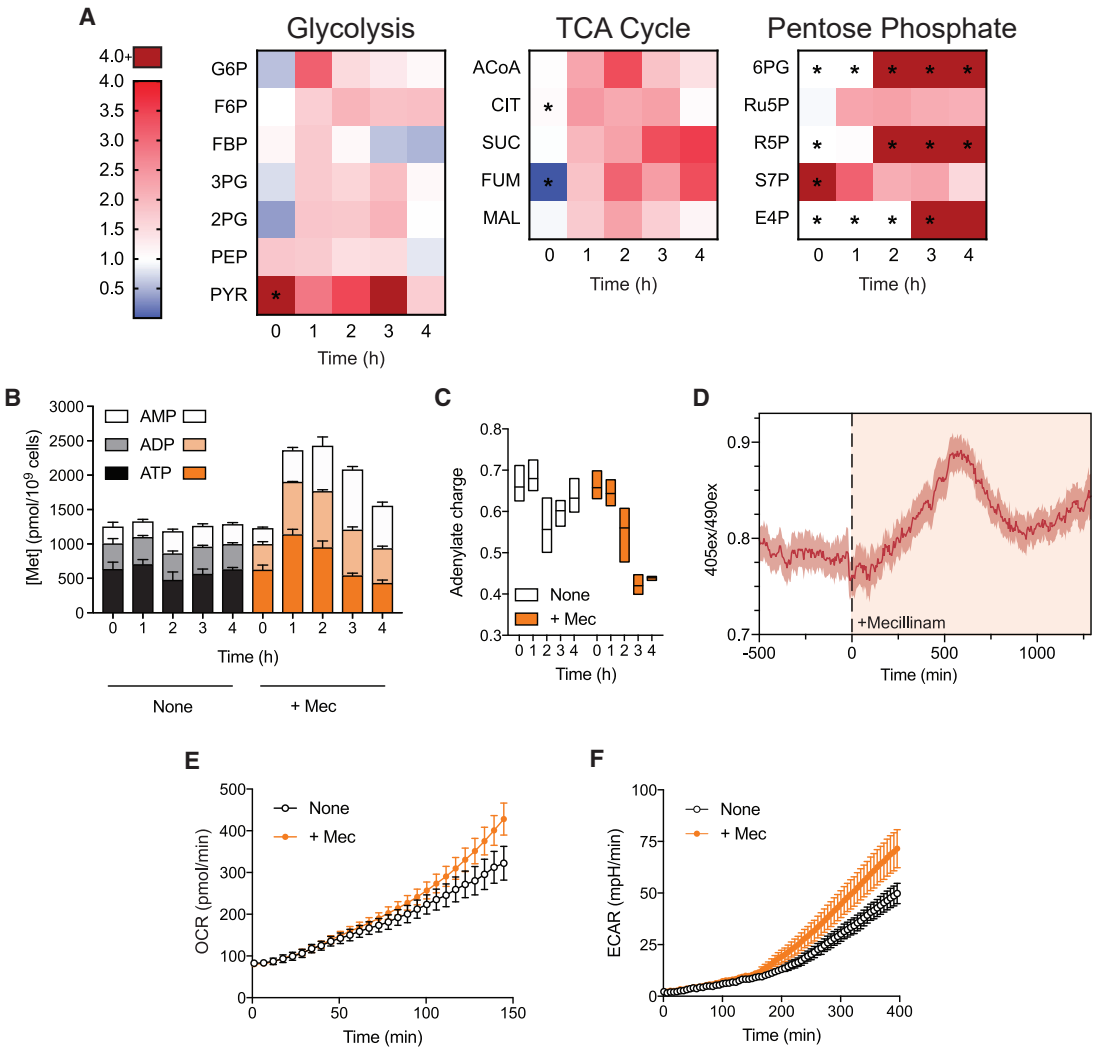

Figure 2. PBP2 inhibition alters activity of central carbon pathways and ATP utilization

(A) Heatmap of time-resolved metabolite concentrations from the major pathways of carbon catabolism. The values indicate concentration in Mec-treated samples relative to untreated controls for cultures grown in M9G. Shown are the means of three biological replicates. Asterisks indicate points where metabolite data were imputed for more than one replicate in a specific treatment condition at that time point.

(B) Time-resolved absolute concentrations of intracellular ATP, ADP, and AMP in untreated and Mec-treated (10 μg/mL) *E. coli*. Shown are the means of three biological replicates. Error bars denote SEM.

(C) Adenylate charge value, calculated as ([ATP] + 0.5[ADP])/([ATP] + [ADP] + [AMP]) in untreated versus Mec-treated *E. coli*. Bars denote the range of values from three biological replicates with the mean indicated by the line within the bars.

(D) Fluorescence ratio (at $405_{ex}/490_{ex}$ nm) of *E. coli* MG1655 expressing QUEEN-2m, a GFP embedded F_1F_0-ATPase. Measurements were made in real time under time-lapse microscopy with cells viewed in a microfluidic device. Data represent the average fluorescence ratio over separate channels observed over 8 h at steady state without antibiotics, followed by 21.5 h after antibiotic addition in M9G medium at 25°C. Shown is the mean of 25 chambers, with shading representing the 95% confidence interval.

(E) Oxygen consumption rate (OCR) of Mec-treated versus untreated *E. coli* measured on a Seahorse XFe extracellular flux analyzer in M9G. Shown are the means of octuplicate technical replicates, which are representative of at least three independent experiments. Error bars denote SEM.

(F) Extracellular acidification rate (ECAR) of Mec-treated versus untreated *E. coli* by Seahorse extracellular flux analyzer in M9G. Shown are the means of octuplicate technical replicates, which are representative of at least three independent experiments. Error bars denote SEM.

See also Figures S2 and S3; Video S1.

metabolites. Thus, we explored the dynamic changes in intracellular ATP, ADP, and AMP in response to mecillinam treatment in M9G compared with untreated *E. coli* within the metabolomics dataset. While untreated cells maintained consistent time-resolved adenylate levels, mecillinam treatment stimulated increases in total adenylate levels within 1 h post treatment that were led by an increase in ATP levels (Figure 2B). Over time, ATP levels declined and were replaced sequentially by elevated ADP levels and then AMP levels (Figure S2). We also assessed the adenylate charge ratio, a measure of total available energy currency of the cell (Chapman et al., 1971), and found that this ratio declined after treatment with mecillinam compared with

Please cite this article in press as: Lobritz et al., Increased energy demand from anabolic-catabolic processes drives β-lactam antibiotic lethality, Cell Chemical Biology (2021), https://doi.org/10.1016/j.chembiol.2021.12.010

the untreated control, suggesting that mecillinam-treated cells become energy starved (Figure 2C).

Given the rapid turnover rate of intracellular ATP, we next sought to obtain measurements with improved kinetic resolution of ATP dynamics in response to mecillinam treatment in M9G. To accomplish this, we used microfluidics to measure real-time relative intracellular ATP concentrations with the ratiometric cellular biosensor, QUEEN-2m (Yaginuma et al., 2014). Since this sensor functions optimally at reduced temperatures (Yaginuma et al., 2014), experiments with this sensor were conducted at 25°C in order to obtain sufficient signal. We expressed QUEEN-2m in *E. coli* and measured the fluorescence signal at two excitation wavelengths to calculate a ratio, denoted $405_{ex}/490_{ex}$, which increases as ATP concentration increases. As expected, steady-state ATP concentration levels of *E. coli* grown without drug exposure were stable. In contrast, exposure of cells to mecillinam resulted in an increase in $405_{ex}/490_{ex}$ signal, indicating an increase in ATP concentration levels consistent with our metabolomics data (Figure 2D and Video S1), although the timescales of these changes are not directly comparable due to the difference in incubation temperature. It is also interesting to note that a dip in signal is observed after the initial peak around 500 min, which is qualitatively similar to the peak-dip behavior observed in the metabolomics data for ATP (Figure S2).

E. coli can generate ATP efficiently through oxidative phosphorylation by coupling carbon oxidation to the formation of redox equivalents to generate a proton-motive force at the electron transport chain, or alternatively through low-efficiency means by mixed-acid fermentation. Having observed augmented energy availability and direct changes in ATP concentrations, we examined whether metabolic pathways for ATP production are perturbed in response to PBP2 inhibition by mecillinam. Using oxygen consumption rate as a proxy, we measured rates of bacterial cellular respiration in M9G using the Seahorse extracellular flux analyzer system. Consistent with the metabolomics and ATP biosensor data, as well as our previous respiratory measurements involving bactericidal antibiotic challenge (Dwyer et al., 2014; Lobritz et al., 2015), mecillinam exposure increased the rates of bacterial cellular respiration (Figure 2E).

We also observed increased rates of extracellular acidification in response to mecillinam treatment over longer time periods (Figure 2F). As this acidification could come from multiple sources, we measured extracellular metabolite production rates of major fermentation products in M9G. We observed increases in acetate production when controlled for population size, as could be seen under conditions of elevated overflow metabolism due to TCA cycle stress (Figure S3A) (Basan et al., 2015). We also found increased secretion rates of the mixed-acid fermentation products, formate and lactate, in response to mecillinam treatment (Figure S3A). In contrast, exposure to chloramphenicol, which suppressed glucose uptake, reduced acetate, formate, and lactate secretion (Figure S3B). Together, our results point to the engagement of multiple pathways of ATP generation in *E. coli* induced by mecillinam treatment, including the involvement of low-efficiency catabolic pathways.

PG synthesis pathway is a source of anabolic demand

The formation of a futile cycle of PG synthesis and degradation in response to mecillinam treatment (Cho et al., 2014) would require increased production of PG precursors. We examined the metabolomics dataset to assess the impact of mecillinam treatment in M9G on the PG synthesis pathway. The glycolytic metabolite fructose-6-phosphate (F6P) is a branchpoint between PG biosynthesis and the glycolytic pathway. At this point, F6P reacts with glutamine to form glucosamine-6-phosphate, the first committed step in the cytoplasmic formation of PG (Figure 3A). In our dataset, we observed elevated quantities of F6P in mecillinam-treated cells (Figure 3A). Furthermore, mecillinam treatment led to increased abundance of all cytoplasmic precursors along the PG biosynthetic pathway through UDP-GlcNAc (Figure 3A), consistent with the model that mecillinam treatment shunts carbon into PG biosynthesis (Cho et al., 2014; Uehara and Park, 2008).

We next sought to evaluate the bioenergetic consequences of PBP2 inhibition by chemically uncoupling mecillinam binding from PG dysregulation. Like mecillinam, treatment with the compound A22 inhibits cell elongation, causing sphere formation (Iwai et al., 2002). However, instead of targeting PBP2, A22 inhibits filament formation of the actin-like protein MreB, blocking PG synthesis by the Rod system (Gitai et al., 2005; Typas et al., 2011; Uehara and Park, 2008). Due to this activity, co-treatment with A22 and mecillinam halts the mecillinam-induced futile cycle and, as observed previously, also results in a loss of lethality in rich media compared with mecillinam treatment alone (Figure 3B) (Cho et al., 2014). We hypothesized that A22 co-treatment with mecillinam would impact the downstream metabolic consequences of mecillinam treatment by interrupting the PG futile cycle. We assessed rates of cellular respiration, mixed-acid fermentation, and glucose utilization (as a proxy for ATP production) in response to mecillinam and A22 treatment in M9G. Co-treatment of A22 with mecillinam resulted in normalization of cellular respiration rate, extracellular acidification rate, and glucose consumption compared with controls (Figure 3C). These data suggest that PG biosynthesis is an important source of metabolic demand in response to mecillinam treatment.

PBP2 inhibition alters amino acid metabolism and increases protein biosynthesis

Mecillinam induces metabolic shifts in response to enzymatic inhibition of PBP2 that are measurable in minimal defined media; however, these shifts appear necessary but not sufficient for mecillinam lethality. We sought to understand differences in rich versus minimal media that may facilitate lethality of PBP2 inhibition. Within the metabolomics dataset, we noted that amino acid and nucleobase metabolism was significantly perturbed in response to mecillinam treatment in M9G (Figure 1D). Mecillinam treatment resulted in increases in the abundance of nearly all amino acids within the first 2 h post treatment (Figure 4A). A notable difference between rich media conditions, where mecillinam is bactericidal, and M9G, where mecillinam is bacteriostatic, is the availability of amino acids and nucleotide precursors. Importantly, the addition of macromolecule precursors to minimal media is sufficient to catalyze lethality (Figure 4B). We thus hypothesized that the underlying toxicity differences in rich and minimal media relate to varying rates of macromolecule synthesis, and that limitations in the rate of protein translation when amino acid precursors are limiting ultimately work as a rheostat to tune overall metabolic demand.

Please cite this article in press as: Lobritz et al., Increased energy demand from anabolic-catabolic processes drives β-lactam antibiotic lethality, Cell Chemical Biology (2021), https://doi.org/10.1016/j.chembiol.2021.12.010

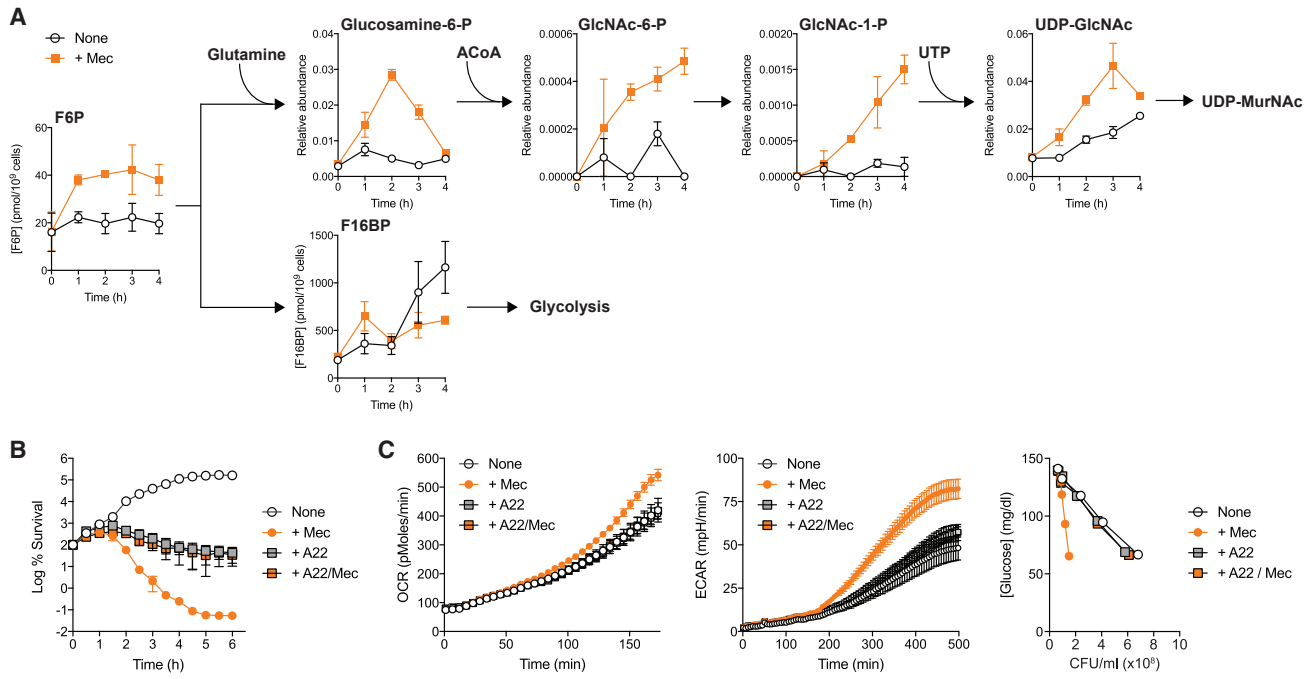

Figure 3. PG synthesis pathway is a source of anabolic demand

(A) Time-resolved absolute and relative concentrations of metabolites in the cytoplasmic PG biosynthetic pathway in untreated and Mec-treated *E. coli*. Shown are the means of three biological replicates for metabolites with absolute concentrations and two biological replicates for metabolites with relative abundances, respectively. Error bars denote SEM.

(B) Time-kill kinetics of Mec- and A22-treated cells compared with untreated and a combination treatment with the two drugs grown in LB medium. Shown are the means of three biological replicates. Error bars denote SEM.

(C) OCR (left), ECAR (middle), and extracellular glucose concentration analysis (right) of Mec- and A22-treated cells compared with untreated conditions and a combination treatment with the two drugs. OCR and ECAR data represent means of octuplicate technical replicates, which are representative of at least three independent experiments. Error bars denote SEM. Extracellular glucose concentration data are the means of three biological replicates. Error bars denote SEM.

To address this hypothesis, we assessed the basal metabolic load of *E. coli* cultured in a variety of different media conditions and observed an increase in oxygen consumption rate that corresponded with conditions that enabled mecillinam lethality (Figure 4C). We next assessed the effect of limiting protein synthesis on the toxicity of mecillinam. Inhibition of translation by co-treatment of cells grown in LB with mecillinam and the translation inhibitor chloramphenicol resulted in attenuation of the lethal effect of mecillinam (Figure 4D). This finding is consistent with previously reported antagonism between bactericidal antibiotics and bacteriostatic protein translation inhibitors that was observed in conjunction with deceleration of cellular respiration, suggesting that protein synthesis is a factor in mecillinam lethality (Lobritz et al., 2015).

Protein synthesis is a major consumer of ATP during normal bacterial homeostasis. We hypothesized that PBP2 inhibition by mecillinam may indirectly impact protein synthesis as a basis for the changes in amino acid abundance observed in the metabolomics dataset. To test this hypothesis, we measured protein synthesis rate in response to mecillinam using a Click-iT labeled fluorescent methionine incorporation assay. First, we developed the assay using a rich medium with defined concentrations of amino acids and nucleobases (MOPS EZ-Rich). Cells were pulsed with a labeled methionine analog and exposed to mecillinam for varying time periods in 3-(N-morpholino)propanesulfonic acid (MOPS) medium with an amino acid supplement lacking methionine. In this system, mecillinam treatment resulted in increased methionine incorporation rates relative to untreated control cells in 1 h and a 5-fold increase in methionine incorporation at 2 h post treatment, when cells begin to die in rich media systems (Figures 1A and 4E). Stimulation of methionine incorporation by mecillinam in *E. coli* was dose dependent and occurred at lethal concentrations (Figure S4). As a control for the assay, methionine incorporation was measured in response to the protein translation inhibitor chloramphenicol. As expected, chloramphenicol treatment resulted in dose-dependent decreases in methionine incorporation relative to untreated control cells (Figure S4).

We next evaluated the impact of media richness on the mecillinam-induced effect on protein translation rate. We compared methionine incorporation rates at steady state and under mecillinam treatment in M9G. While M9G supplementation with amino acids or amino acids and nucleobases resulted in increased labeled methionine incorporation in response to mecillinam treatment, methionine incorporation rates were unchanged in M9G or M9G plus nucleobases in response to mecillinam treatment (Figure 4F). Thus, mecillinam treatment induces increased protein synthesis rates in conditions where amino acids are not limiting and the antibiotic is bactericidal. On the other hand, in media conditions where amino acid availability is limited and the drug is bacteriostatic, mecillinam treatment fails to increase protein synthesis rates.

Please cite this article in press as: Lobritz et al., Increased energy demand from anabolic-catabolic processes drives β-lactam antibiotic lethality, Cell Chemical Biology (2021), https://doi.org/10.1016/j.chembiol.2021.12.010

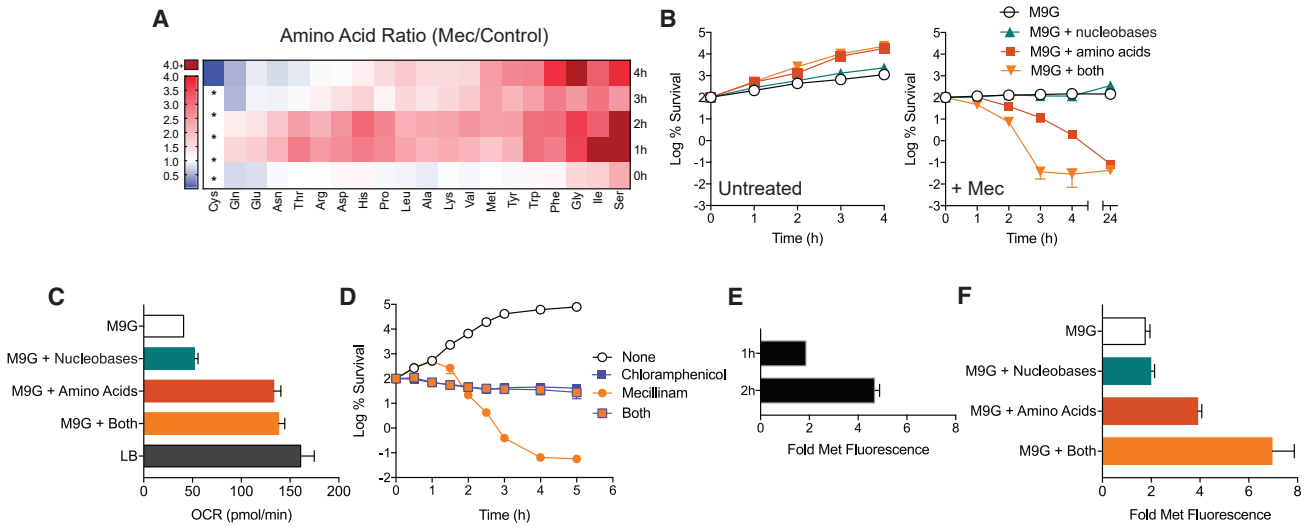

Figure 4. PBP2 inhibition alters amino acid metabolism and increases protein biosynthesis

(A) Heatmap of time-resolved metabolite concentrations of amino acids. The values indicate concentration in Mec-treated samples relative to untreated controls for cultures grown in M9G. Shown are the means of three biological replicates. Asterisks indicate points where metabolite data were imputed for more than one replicate in a specific treatment condition at that time point.

(B) Time-kill kinetics of untreated (left) and Mec-treated (right) cells with supplementation with pooled nucleobases, amino acids, or both. Shown are the means of three biological replicates. Error bars denote SEM.

(C) OCR of *E. coli* growing in LB and M9G media supplemented with pooled nucleobases, amino acids, or both. Shown are the means of octuplicate technical replicates, which are representative of at least three independent experiments. Error bars denote SEM.

(D) Time-kill kinetics of Mec- and Cam-treated cells compared with untreated conditions and a combination treatment with the two drugs. Shown are the means of three biological replicates. Error bars denote SEM.

(E) Fold change in Click-iT fluorescent methionine incorporation assay between untreated and Mec-treated cells at 1 h and 2 h after treatment. Shown are the means of six biological replicates. Error bars denote SEM.

(F) Fold change in methionine fluorescence of Mec-treated cells grown in M9G supplemented with pooled nucleobases, amino acids, or both, and treated for 2 h. Shown are the means of six biological replicates. Error bars denote SEM.

See also Figure S4.

Mecillinam treatment results in a dysregulated cellular redox environment

Intracellular redox alterations have been previously identified in response to β-lactam antibiotic treatment in *E. coli* (Belenky et al., 2015; Dwyer et al., 2014; Kohanski et al., 2007); however, these prior studies have been limited by the use of the pan-PBP inhibitor ampicillin, which induces both lytic and non-lytic forms of cell death. Given the impact of mecillinam treatment on intracellular energy stores (Figure 2B) and cellular respiration (Figure 2E), we examined the impact of PBP2 inhibition in M9G on redox balance within the metabolomics dataset. In this system, NAD^+ levels were significantly elevated in bacteria treated with mecillinam while NADH levels remained stable, consistent with a shift in the oxidation state of the cells. Similar changes were observed in the pools of oxidized co-factors flavin adenine dinucleotide (FAD) and flavin mononucleotide (FMN) (Figure 5A). Increased quantities of $NADP^+$ relative to NADPH were also identified, consistent with the observed increase in anabolic reactions within the cell (Figure 5A). Increased levels of methionine sulfoxide were observed in response to mecillinam treatment (Figure 5B), a known biomarker of cellular oxidation (Levine et al., 1996). Overall, the metabolomic profile observed is consistent with metabolic changes associated with an oxidized cellular redox environment in response to PBP2 inhibition.

Redox-related changes from metabolic demand induced by antibiotic drug-target interactions have been hypothesized to be a causative contributor in bacterial cell death in a range of bactericidal antibiotics, including pan-PBP inhibitors such as ampicillin. If PBP2 inhibition leads to similar redox-related lethal effects, the use of a scavenger for reactive metabolic by-products should attenuate mecillinam lethality. As has been demonstrated previously (Dwyer et al., 2014; Lopatkin et al., 2019; Wong et al., 2021), the antioxidant glutathione can effectively attenuate antibiotic killing. Accordingly, to test the above hypothesis, we co-treated cells grown in rich media with mecillinam and 10 mM glutathione. Importantly, under the experimental conditions tested, glutathione does not react with mecillinam or impact mecillinam uptake (Figure S5). We found that co-treatment with glutathione resulted in the attenuation of killing with mecillinam (Figure 5C), indicating that the metabolic and redox changes observed in response to mecillinam treatment in the metabolomics dataset are causative contributors to mecillinam-induced lethality.

DISCUSSION

In this work, we examined the metabolic consequences of the enzymatic inhibition of a key antibiotic target, PBP2, by the β-lactam antibiotic mecillinam. We found that inhibition of PBP2 by mecillinam results in altered cellular catabolic and anabolic processes, including increased abundance of metabolites in energy-generating pathways, the PG synthesis pathway,

Please cite this article in press as: Lobritz et al., Increased energy demand from anabolic-catabolic processes drives β-lactam antibiotic lethality, Cell Chemical Biology (2021), https://doi.org/10.1016/j.chembiol.2021.12.010

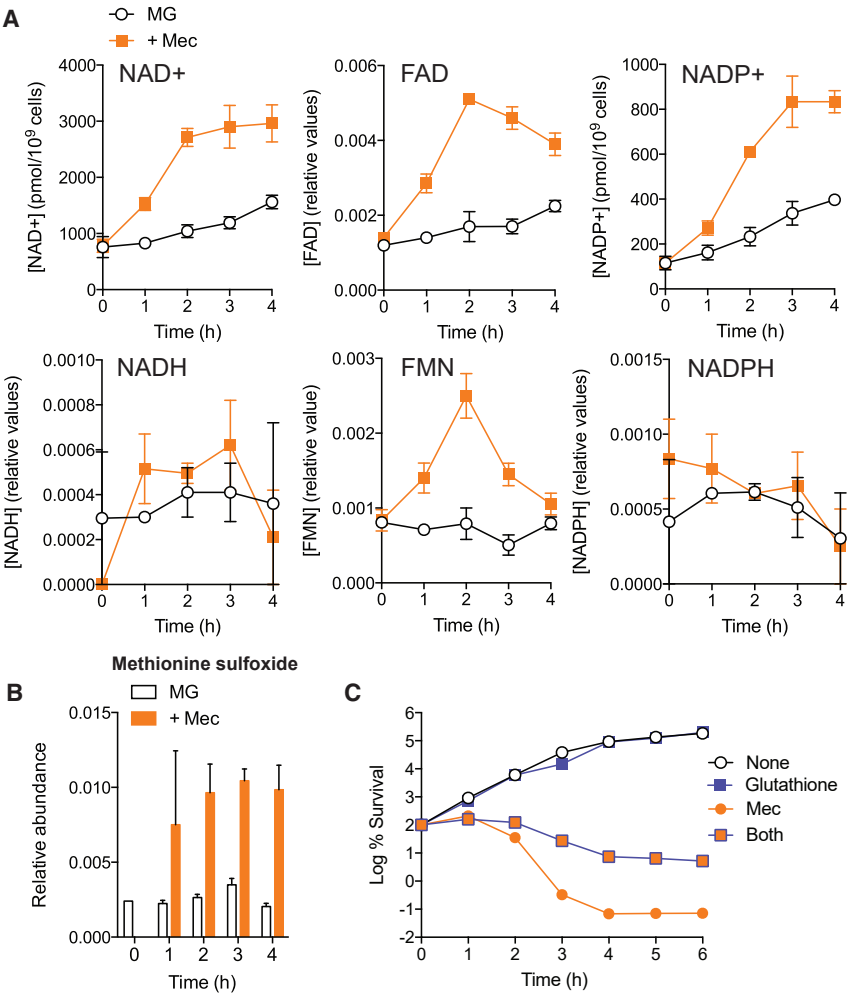

Figure 5. Mecillinam treatment results in a dysregulated cellular redox environment

(A) Time-resolved absolute concentrations of intracellular NAD^+ and $NADP^+$ and relative concentrations of NADH, NADPH, FAD, and FMN in untreated and Mec-treated (10 μg/mL) *E. coli* MG1655. Shown are the means of three biological replicates for metabolites with absolute concentrations and two biological replicates for metabolites with relative abundances, respectively. Error bars denote SEM.

(B) Time-resolved relative abundance of methionine sulfoxide in untreated and Mec-treated *E. coli*. Shown are the means of two biological replicates. Error bars denote SEM.

(C) Time-kill kinetics of Mec- and glutathione-treated cells compared with untreated conditions and a combination treatment with both compounds. Shown are the means of three biological replicates. Error bars denote SEM.

See also Figure S5.

and amino acid and nucleotide synthesis pathways. We further showed that, in the context of the metabolic changes induced by PBP2 inhibition, the availability of exogenous amino acids to support antibiotic-induced accelerations in protein synthesis, and the presence of reactive metabolic by-products, are important factors in mecillinam lethality. Together, these data support a model of β-lactam-induced lethality in which inhibition of the PBP drug target serves as a critical first step to drive an imbalance between normal anabolic-catabolic homeostasis, and that this toxic shift in metabolic demand is a critical factor in antibiotic lethality.

Mecillinam blocks lateral cell wall elongation and results in spheroplast formation followed by eventual cell death via inhibition of PBP2 (Spratt, 1977; Tybring and Melchior, 1975), an enzyme that catalyzes transpeptidation of PG strands in *E. coli* (Ishino et al., 1982). Early observations of mecillinam resistance identified mutations that were associated with an induction of the stringent response; however, the precise mechanism underlying this resistance has remained unclear (Joseleau-Petit et al., 1994; Lai et al., 2017; Thulin et al., 2015; Vinella et al., 1992, 1996). PBP2 has also been found to be nonessential in conditions under which the division protein FtsZ is overproduced (Vinella et al., 1993). This observation was utilized to show that PBP2 inhibition is lethal even in conditions where PBP2 is nonessential and that this lethality extends from a futile cycle of PG synthesis and degradation (Cho et al., 2014). An important question remaining from this earlier work was how these target-proximal effects of antibiotic treatment might be connected to the corruption of downstream metabolic processes that have been implicated in the lethality of bactericidal antibiotics (Belenky et al., 2015; Dwyer et al., 2014; Foti et al., 2012; Hong et al., 2019; Kohanski et al., 2007; Stokes et al., 2019). Notably, a recent study investigating β-lactam treatment and L-form growth of Gram-positive bacteria found that β-lactam treatment induced increased glycolytic flux and production of reactive oxygen species (Kawai et al., 2019). Consistent with the present study, this metabolic response was shown to be important to the non-lytic killing of these bacteria by β-lactam antibiotics (Kawai et al., 2019). Our results build on this body of work by expanding our understanding of the metabolic impacts of β-lactam treatment, encompassing both the target-proximal and downstream effects of PBP2 inhibition.

Under balanced growth, *E. coli* must distribute carbon among pathways designated for biomass production and energy generation. Carbon oxidation rates are coupled both to ATP demand and to the efficiency of the metabolic process: low metabolic efficiency is achieved through fermentation and higher metabolic efficiency is generated through cellular respiration pathways (Basan et al., 2015). Our observations on cellular adenylate charge (Figure 2C) suggest that mecillinam treatment creates a condition in which the cells are starved for ATP. Attempts to mitigate this anabolic energetic demand by increasing catabolic rates appear to be involved in the ultimate result of cell death. Increased metabolic demand can lead to the production of reactive oxygen species, which oxidize cellular components including proteins and nucleotide pools (Foti et al., 2012;

Please cite this article in press as: Lobritz et al., Increased energy demand from anabolic-catabolic processes drives β-lactam antibiotic lethality, Cell Chemical Biology (2021), https://doi.org/10.1016/j.chembiol.2021.12.010

Gonzalez-Flecha and Demple, 1995; Gruber and Walker, 2018; Imlay, 2003; Van Acker and Coenye, 2017).

The finding of accelerated protein synthesis in response to mecillinam was unexpected. When proteostasis is perturbed, a coordinated cellular response ensues (Powers et al., 2012; Santra et al., 2018), which is likely a metabolically demanding cellular event (Stouthamer, 1973). Perturbations to proteostasis have been linked to antibiotic mechanisms of action, including the induction of protein aggregates by aminoglycosides (Kohanski et al., 2008; Ling et al., 2012) and as a general prospect for antibiotic development (Lupoli et al., 2018). We observed oxidation of the methionine amino acid pool, consistent with previous findings of oxidation of the broader proteome (Belenky et al., 2015), suggesting a possible explanation for the increase in protein synthesis rates in response to mecillinam treatment. It is also possible that some of these induced proteins could contribute to the lethal effects of antibiotic treatment. For instance, incomplete base excision repair resulting in part from increased expression of the DNA glycosylase *mutM* was shown to contribute to the lethality of oxidative stress stimulated by MalE-LacZ induction (Gruber and Walker, 2018; Takahashi et al., 2017). Analyzing the proteome-wide response to PBP2 inhibition could provide additional insight into this phenomenon.

The experimental measurement of metabolomic responses to antibiotics in bacteria requires trade-off decisions. Here, we chose to take metabolic measurements in nonlethal (bacteriostatic) media conditions, which provided greater confidence that changes in metabolite levels are the direct result of enzymatic inactivation of PBP2 rather than nonspecific by-products of cell death. In this context, it is possible that metabolic shifts measured in bacteriostatic media conditions may not translate precisely to the lethal (bactericidal) media conditions. We sought to address this potential liability by testing key attributions made from our metabolomics dataset in a bactericidal context where possible. In support of this, we observed metabolic shifts in bacteriostatic conditions, such as accelerated respiration, that have been previously linked to cell killing (Stokes et al., 2019), and the responses observed following mecillinam treatment differed significantly from those observed following treatment with the translation inhibitor chloramphenicol. Based on the finding that macromolecule precursor supplementation resulted in elevated respiration and protein synthesis, we hypothesize that core metabolic responses are conserved in both bacteriostatic and bactericidal conditions for mecillinam, but that a critical threshold must be reached in order for these metabolic changes to result in cell death. While a similar phenomenon has been observed with intracellular ATP levels (Lopatkin et al., 2019; Shan et al., 2017), additional investigation is needed to more precisely understand this transition to death in varying metabolic contexts.

Our study contributes to a developing understanding of the role that bacterial metabolism plays in antibiotic efficacy and how these insights could be utilized to develop improved antibacterial therapeutic strategies (Defraine et al., 2018; Meylan et al., 2018; Stokes et al., 2019; Van Acker and Coenye, 2017). For example, co-treatment outcomes using mecillinam and chloramphenicol demonstrate the potential of these data to inform the development of rational antibiotic combinations. Additionally, recent work has explored how bacterial growth media that more closely mimic physiologic conditions can impact the efficacy of antibiotics (Carfrae et al., 2020; Weber et al., 2020). Future work should seek to expand the metabolomic analysis conducted here to alternative growth conditions with the goal of understanding how the metabolic context of human infection impacts antibiotic effects. Similarly, it will be important to consider how metabolic changes may differ between antibiotic-sensitive and antibiotic-resistant bacterial pathogens. For example, in a recent study the mecillinam resistome was characterized using transposon insertion sequencing to generate a large number of mecillinam-resistant mutants (Lai et al., 2017). Metabolomic profiling of a selection of strains from this collection could improve our understanding of metabolic changes within the context of mechanistically diverse resistant mutants. Such approaches could help bridge *in vitro*-derived metabolic observations to clinically useful information for designing novel therapeutic strategies.

While drug-target interaction of β-lactam antibiotics with cognate PBPs has been understood for some time, advances continue to be made on the broader cellular consequences of β-lactam treatment. Our data link the finding that PBP inhibition leads to dysregulation of the bacterial cell wall synthesis machinery (Cho et al., 2014; Uehara and Park, 2008) to specific toxic downstream metabolic consequences, including redox stresses associated with bacterial cell death (Belenky et al., 2015; Dwyer et al., 2014; Foti et al., 2012; Kohanski et al., 2007). In our effort to combat the growing antibiotic resistance crisis, further investigation of our antibiotic armamentarium, including essential classes of drugs such as the β-lactams, is critical both for the discovery of new antibiotics and for the rational use of existing ones.

SIGNIFICANCE

β-Lactam antibiotics have been a preferred first-line therapy for the treatment of bacterial infections since they became broadly available in the 1940s. Remarkably, new insights into the mode of action of β-lactams continue to be made as we increase our understanding of bacterial outer membrane biogenesis. This includes the recent identification that β-lactams induce a futile cycle of peptidoglycan (PG) synthesis and degradation as a core aspect of their lethal effect on bacteria. Here, we applied a metabolomics approach to identify perturbations induced by the β-lactam antibiotic mecillinam in the Gram-negative bacterial pathogen *Escherichia coli*. PBP2 inhibition by mecillinam results in broad metabolic shifts of multiple anabolic and catabolic processes, including alterations to PG and protein biosynthesis. Alongside this shift, we observed alterations in glycolytic activity and ATP utilization and a broadly dysregulated cellular redox environment. Importantly, scavenging of reactive metabolic by-products attenuates drug-induced lethality. Taken together, this work links the target-proximal effects of PG dysregulation with downstream metabolic phenomena, including redox dysregulation, that cumulatively result in bacterial cellular death.

STAR★METHODS

Detailed methods are provided in the online version of this paper and include the following:

SUPPLEMENTAL INFORMATION

Supplemental information can be found online at https://doi.org/10.1016/j.chembiol.2021.12.010.

ACKNOWLEDGMENTS

We are grateful to Tom Bernhardt for important discussions impacting the design of the study and critical feedback on the manuscript. We thank Charles Vidoudez and Sunia A. Trauger at the Harvard Center for Mass Spectrometry for assistance with LC-MS experiments. We also thank Allison Lopatkin and Matt Russo for useful discussions and technical assistance. This work was supported by a grant to J.J.C. from the Defense Threat Reduction Agency (HDTRA1-15-1-0051); support to M.A.L. by the KL2/Catalyst Medical Research Investigator Training award (an appointed KL2 award) from Harvard Catalyst, the Harvard Clinical and Translational Science Center (National Center for Research Resources and the National Center for Advancing Translational Sciences, National Institutes of Health award KL2 TR001100); by fellowships to I.W.A. and S.C.B. from the National Science Foundation Graduate Research Fellowship Program (1122374); by the James S. McDonnell Foundation to F.W.; by National Institutes of Health grant 1R35 GM133759 to G.L.; by National Institutes of Health grant R01CA021615 to G.C.W; and by a generous gift from Anita and Josh Bekenstein. G.C.W. is an American Cancer Society Professor.

AUTHOR CONTRIBUTIONS

Conceptualization, M.A.L., C.B.M.P., and A.G.; methodology, M.A.L., I.W.A., C.B.M.P., D.B., A.G., L.B.G.C., F.W., and G.L.; investigation, M.A.L., I.W.A., D.B., C.B.M.P., A.G., Y.F., L.B.G.C., T.F., S.C.B., F.W., C.G., C.W.B., and G.L.; formal analysis, M.A.L., I.W.A., D.B., C.B.M.P., and A.G.; writing – original draft, M.A.L. and I.W.A.; writing – review and editing, D.B., C.B.M.P., A.G., Y.F., L.B.G.C., F.W., G.L., G.C.W., D.J.D., and J.J.C.; funding acquisition, J.J.C.; resources, J.J.C.; supervision, G.C.W., D.J.D., and J.J.C.

DECLARATION OF INTERESTS

M.A.L. is a full-time employee and shareholder of F. Hoffmann-La Roche, Ltd. J.J.C. is a scientific co-founder and scientific advisory board chair of Enbiotix, an antibiotics discovery company.

Received: June 25, 2021
Revised: October 11, 2021
Accepted: December 6, 2021
Published: January 5, 2022

REFERENCES

Basan, M., Hui, S., Okano, H., Zhang, Z., Shen, Y., Williamson, J.R., and Hwa, T. (2015). Overflow metabolism in *Escherichia coli* results from efficient proteome allocation. Nature *528*, 99–104.

Belenky, P., Ye, J.D., Porter, C.B., Cohen, N.R., Lobritz, M.A., Ferrante, T., Jain, S., Korry, B.J., Schwarz, E.G., Walker, G.C., et al. (2015). Bactericidal antibiotics induce toxic metabolic perturbations that lead to cellular damage. Cell Rep. *13*, 968–980.

Carfrae, L.A., MacNair, C.R., Brown, C.M., Tsai, C.N., Weber, B.S., Zlitni, S., Rao, V.N., Chun, J., Junop, M.S., Coombes, B.K., et al. (2020). Mimicking the human environment in mice reveals that inhibiting biotin biosynthesis is effective against antibiotic-resistant pathogens. Nat. Microbiol. *5*, 93–101.

Chapman, A.G., Fall, L., and Atkinson, D.E. (1971). Adenylate energy charge in *Escherichia coli* during growth and starvation. J. Bacteriol. *108*, 1072–1086.

Cho, H., Uehara, T., and Bernhardt, T.G. (2014). Beta-lactam antibiotics induce a lethal malfunctioning of the bacterial cell wall synthesis machinery. Cell *159*, 1300–1311.

Cho, H., Wivagg, C.N., Kapoor, M., Barry, Z., Rohs, P.D.A., Suh, H., Marto, J.A., Garner, E.C., and Bernhardt, T.G. (2016). Bacterial cell wall biogenesis is mediated by SEDS and PBP polymerase families functioning semi-autonomously. Nat. Microbiol. *1*, 16172.

Christodoulou, D., Link, H., Fuhrer, T., Kochanowski, K., Gerosa, L., and Sauer, U. (2018). Reserve flux capacity in the pentose phosphate pathway enables *Escherichia coli*'s rapid response to oxidative stress. Cell Syst. *6*, 569–578.e7.

Defraine, V., Fauvart, M., and Michiels, J. (2018). Fighting bacterial persistence: current and emerging anti-persister strategies and therapeutics. Drug Resist. Updat. *38*, 12–26.

Delhaye, A., Collet, J.F., and Laloux, G. (2016). Fine-tuning of the cpx envelope stress response is required for cell wall homeostasis in *Escherichia coli*. MBio. *7*, e00047-16.

Dwyer, D.J., Belenky, P.A., Yang, J.H., MacDonald, I.C., Martell, J.D., Takahashi, N., Chan, C.T., Lobritz, M.A., Braff, D., Schwarz, E.G., et al. (2014). Antibiotics induce redox-related physiological alterations as part of their lethality. Proc. Natl. Acad. Sci. U S A *111*, E2100–E2109.

Egan, A.J.F., Errington, J., and Vollmer, W. (2020). Regulation of peptidoglycan synthesis and remodelling. Nat. Rev. Microbiol. *18*, 446–460.

Foti, J.J., Devadoss, B., Winkler, J.A., Collins, J.J., and Walker, G.C. (2012). Oxidation of the guanine nucleotide pool underlies cell death by bactericidal antibiotics. Science *336*, 315–319.

Gitai, Z., Dye, N.A., Reisenauer, A., Wachi, M., and Shapiro, L. (2005). MreB actin-mediated segregation of a specific region of a bacterial chromosome. Cell *120*, 329–341.

Gonzalez-Flecha, B., and Demple, B. (1995). Metabolic sources of hydrogen peroxide in aerobically growing *Escherichia coli*. J. Biol. Chem. *270*, 13681–13687.

Gruber, C.C., and Walker, G.C. (2018). Incomplete base excision repair contributes to cell death from antibiotics and other stresses. DNA Repair *71*, 108–117.

Guest, R.L., and Raivio, T.L. (2016). Role of the gram-negative envelope stress response in the presence of antimicrobial agents. Trends Microbiol. *24*, 377–390.

Hong, Y., Zeng, J., Wang, X., Drlica, K., and Zhao, X. (2019). Post-stress bacterial cell death mediated by reactive oxygen species. Proc. Natl. Acad. Sci. U S A *116*, 10064–10071.

Imlay, J.A. (2003). Pathways of oxidative damage. Annu. Rev. Microbiol. *57*, 395–418.

Ishino, F., Tamaki, S., Spratt, B.G., and Matsuhashi, M. (1982). A mecillinam-sensitive peptidoglycan crosslinking reaction in *Escherichia coli*. Biochem. Biophys. Res. Commun. *109*, 689–696.

Iwai, N., Nagai, K., and Wachi, M. (2002). Novel S-benzylisothiourea compound that induces spherical cells in *Escherichia coli* probably by acting on a rod-shape-determining protein(s) other than penicillin-binding protein 2. Biosci. Biotechnol. Biochem. *66*, 2658–2662.

Joseleau-Petit, D., Thevenet, D., and D'Ari, R. (1994). ppGpp concentration, growth without PBP2 activity, and growth-rate control in *Escherichia coli*. Mol. Microbiol. *13*, 911–917.

Kawai, Y., Mercier, R., Mickiewicz, K., Serafini, A., Sorio de Carvalho, L.P., and Errington, J. (2019). Crucial role for central carbon metabolism in the bacterial L-form switch and killing by beta-lactam antibiotics. Nat. Microbiol. *4*, 1716–1726.

Kohanski, M.A., Dwyer, D.J., Hayete, B., Lawrence, C.A., and Collins, J.J. (2007). A common mechanism of cellular death induced by bactericidal antibiotics. Cell *130*, 797–810.

Kohanski, M.A., Dwyer, D.J., Wierzbowski, J., Cottarel, G., and Collins, J.J. (2008). Mistranslation of membrane proteins and two-component system activation trigger antibiotic-mediated cell death. Cell *135*, 679–690.

Lai, G.C., Cho, H., and Bernhardt, T.G. (2017). The mecillinam resistome reveals a role for peptidoglycan endopeptidases in stimulating cell wall synthesis in *Escherichia coli*. PLoS Genet. *13*, e1006934.

Lambert, G., and Kussell, E. (2015). Quantifying selective pressures driving bacterial evolution using lineage analysis. Phys. Rev. X *5*, 011016.

Laubacher, M.E., and Ades, S.E. (2008). The Rcs phosphorelay is a cell envelope stress response activated by peptidoglycan stress and contributes to intrinsic antibiotic resistance. J. Bacteriol. *190*, 2065–2074.

Levine, R.L., Mosoni, L., Berlett, B.S., and Stadtman, E.R. (1996). Methionine residues as endogenous antioxidants in proteins. Proc. Natl. Acad. Sci. U S A *93*, 15036–15040.

Lindman, M., and Dick, T. (2019). Bedaquiline eliminates bactericidal activity of beta-lactams against *Mycobacterium abscessus*. Antimicrob. Agents Chemother. *63*, e00827-19.

Ling, J., Cho, C., Guo, L.T., Aerni, H.R., Rinehart, J., and Soll, D. (2012). Protein aggregation caused by aminoglycoside action is prevented by a hydrogen peroxide scavenger. Mol. Cell *48*, 713–722.

Lobritz, M.A., Belenky, P., Porter, C.B., Gutierrez, A., Yang, J.H., Schwarz, E.G., Dwyer, D.J., Khalil, A.S., and Collins, J.J. (2015). Antibiotic efficacy is linked to bacterial cellular respiration. Proc. Natl. Acad. Sci. U S A *112*, 8173–8180.

Lopatkin, A.J., Stokes, J.M., Zheng, E.J., Yang, J.H., Takahashi, M.K., You, L., and Collins, J.J. (2019). Bacterial metabolic state more accurately predicts antibiotic lethality than growth rate. Nat. Microbiol. *4*, 2109–2117.

Lupoli, T.J., Vaubourgeix, J., Burns-Huang, K., and Gold, B. (2018). Targeting the proteostasis network for mycobacterial drug discovery. ACS Infect. Dis. *4*, 478–498.

Meeske, A.J., Riley, E.P., Robins, W.P., Uehara, T., Mekalanos, J.J., Kahne, D., Walker, S., Kruse, A.C., Bernhardt, T.G., and Rudner, D.Z. (2016). SEDS proteins are a widespread family of bacterial cell wall polymerases. Nature *537*, 634–638.

Meylan, S., Andrews, I.W., and Collins, J.J. (2018). Targeting antibiotic tolerance, pathogen by pathogen. Cell *172*, 1228–1238.

Miller, C., Thomsen, L.E., Gaggero, C., Mosseri, R., Ingmer, H., and Cohen, S.N. (2004). SOS response induction by beta-lactams and bacterial defense against antibiotic lethality. Science *305*, 1629–1631.

Moreillon, P., Markiewicz, Z., Nachman, S., and Tomasz, A. (1990). Two bactericidal targets for penicillin in pneumococci: autolysis-dependent and autolysis-independent killing mechanisms. Antimicrob. Agents Chemother. *34*, 33–39.

Powers, E.T., Powers, D.L., and Gierasch, L.M. (2012). FoldEco: a model for proteostasis in *E. coli*. Cell Rep. *1*, 265–276.

Santra, M., Dill, K.A., and de Graff, A.M.R. (2018). How do chaperones protect a cell's proteins from oxidative damage? Cell Syst. *6*, 743–751.e3.

Shan, Y., Brown Gandt, A., Rowe, S.E., Deisinger, J.P., Conlon, B.P., and Lewis, K. (2017). ATP-dependent persister formation in *Escherichia coli*. mBio *8*, e02267-16.

Shetty, A., and Dick, T. (2018). Mycobacterial cell wall synthesis inhibitors cause lethal ATP burst. Front. Microbiol. *9*, 1898.

Spratt, B.G. (1975). Distinct penicillin binding proteins involved in the division, elongation, and shape of *Escherichia coli* K12. Proc. Natl. Acad. Sci. U S A *72*, 2999–3003.

Spratt, B.G. (1977). The mechanism of action of mecillinam. J. Antimicrob. Chemother. *3*, 13–19.

Spratt, B.G., and Cromie, K.D. (1988). Penicillin-binding proteins of gram-negative bacteria. Rev. Infect. Dis. *10*, 699–711.

Stokes, J.M., Lopatkin, A.J., Lobritz, M.A., and Collins, J.J. (2019). Bacterial metabolism and antibiotic efficacy. Cell Metab. *30*, 251–259.

Stouthamer, A.H. (1973). A theoretical study on the amount of ATP required for synthesis of microbial cell material. Antonie Van Leeuwenhoek. *39*, 545–565.

Takahashi, N., Gruber, C.C., Yang, J.H., Liu, X., Braff, D., Yashaswini, C.N., Bhubhanil, S., Furuta, Y., Andreescu, S., Collins, J.J., et al. (2017). Lethality of MalE-LacZ hybrid protein shares mechanistic attributes with oxidative component of antibiotic lethality. Proc. Natl. Acad. Sci. U S A *114*, 9164–9169.

Thulin, E., Sundqvist, M., and Andersson, D.I. (2015). Amdinocillin (Mecillinam) resistance mutations in clinical isolates and laboratory-selected mutants of *Escherichia coli*. Antimicrob. Agents Chemother. *59*, 1718–1727.

Tybring, L., and Melchior, N.H. (1975). Mecillinam (FL 1060), a 6beta-amidinopenicillanic acid derivative: bactericidal action and synergy in vitro. Antimicrob. Agents Chemother. *8*, 271–276.

Typas, A., Banzhaf, M., Gross, C.A., and Vollmer, W. (2011). From the regulation of peptidoglycan synthesis to bacterial growth and morphology. Nat. Rev. Microbiol. *10*, 123–136.

Uehara, T., and Park, J.T. (2008). Growth of *Escherichia coli*: significance of peptidoglycan degradation during elongation and septation. J. Bacteriol. *190*, 3914–3922.

Van Acker, H., and Coenye, T. (2017). The role of reactive oxygen species in antibiotic-mediated killing of bacteria. Trends Microbiol. *25*, 456–466.

Vinella, D., D'Ari, R., Jaffe, A., and Bouloc, P. (1992). Penicillin binding protein 2 is dispensable in *Escherichia coli* when ppGpp synthesis is induced. EMBO J. *11*, 1493–1501.

Vinella, D., Gagny, B., Joseleau-Petit, D., D'Ari, R., and Cashel, M. (1996). Mecillinam resistance in *Escherichia coli* is conferred by loss of a second activity of the AroK protein. J. Bacteriol. *178*, 3818–3828.

Vinella, D., Joseleau-Petit, D., Thevenet, D., Bouloc, P., and D'Ari, R. (1993). Penicillin-binding protein 2 inactivation in *Escherichia coli* results in cell division inhibition, which is relieved by FtsZ overexpression. J. Bacteriol. *175*, 6704–6710.

Weber, B.S., De Jong, A.M., Guo, A.B.Y., Dharavath, S., French, S., Fiebig-Comyn, A.A., Coombes, B.K., Magolan, J., and Brown, E.D. (2020). Genetic and chemical screening in human blood serum reveals unique antibacterial targets and compounds against *Klebsiella pneumoniae*. Cell Rep. *32*, 107927.

Wong, F., Stokes, J.M., Cervantes, B., Penkov, S., Friedrichs, J., Renner, L.D., and Collins, J.J. (2021). Cytoplasmic condensation induced by membrane damage is associated with antibiotic lethality. Nat. Commun. *12*, 2321.

Yaginuma, H., Kawai, S., Tabata, K.V., Tomiyama, K., Kakizuka, A., Komatsuzaki, T., Noji, H., and Imamura, H. (2014). Diversity in ATP concentrations in a single bacterial cell population revealed by quantitative single-cell imaging. Sci. Rep. *4*, 6522.

Yousif, S.Y., Broome-Smith, J.K., and Spratt, B.G. (1985). Lysis of *Escherichia coli* by beta-lactam antibiotics: deletion analysis of the role of penicillin-binding proteins 1A and 1B. J. Gen. Microbiol. *131*, 2839–2845.

Please cite this article in press as: Lobritz et al., Increased energy demand from anabolic-catabolic processes drives β-lactam antibiotic lethality, Cell Chemical Biology (2021), https://doi.org/10.1016/j.chembiol.2021.12.010

STAR★METHODS

KEY RESOURCES TABLE

REAGENT or RESOURCE	SOURCE	IDENTIFIER
Bacterial and virus strains		
Escherichia coli MG1655	ATCC	ATCC# 700926
Chemicals, peptides, and recombinant proteins		
Mecillinam	Sigma-Aldrich	Cat# 33447
Chloramphenicol	Sigma-Aldrich	Cat# C0378
A22 hydrochloride	Sigma-Aldrich	Cat# SML0471
L-Glutathione reduced	Sigma-Aldrich	Cat# G4251
Poly-D-lysine	Sigma-Aldrich	Cat# P6407
Click-iT HPG	Thermo Fisher Scientific	Cat# C10186
Alexa Fluor 488 Azide	Thermo Fisher Scientific	Cat# A10266
Acetonitrile	Sigma-Aldrich	Cat# 271004
B-PER II	Thermo Fisher Scientific	Cat# 78260
Lysozyme	Sigma-Aldrich	Cat# L6876
DNase I	Thermo Fisher Scientific	Cat# 90083
Ampicillin-d_5	Cayman Chemical Company	Cat# 25356
Critical commercial assays		
Glucose Colorimetric Assay Kit	Cayman Chemical Company	Cat# 10009582
Acetate Colorimetric Assay Kit	Sigma-Aldrich	Cat# MAK086
Formate Colorimetric Assay Kit	Sigma-Aldrich	Cat# MAK059
D-Lactate Colorimetric Assay Kit	Sigma-Aldrich	Cat# MAK058
Seahorse XFe96 FluxPak	Agilent Technologies	Cat# 102416
Click-iT Cell Reaction Buffer Kit	Thermo Fisher Scientific	Cat# C10269
Pierce Coomassie Plus Assay Kit	Thermo Fisher Scientific	Cat# 23236
Recombinant DNA		
Plasmid: Prpsl::QUEEN-2m	(Yaginuma et al., 2014)	N/A
Software and algorithms		
Matlab R2014b	The MathWorks, Inc.	https://www.mathworks.com/products/matlab.html
FlowJo	BD	https://www.flowjo.com

RESOURCE AVAILABILITY

Lead contact

Further information and requests for resources and reagents should be directed to James J. Collins (jimjc@mit.edu).

Materials availability

This study did not generate new unique reagents.

Data and code availability

- All data supporting this study are available from the lead contact upon request.
- This study did not generate new code.
- Any additional information required to reanalyze the data reported in this paper is available from the lead contract upon request.

EXPERIMENTAL MODEL AND SUBJECT DETAILS

E. coli MG1655 was used as the experimental model for all experiments. Experiments were conducted at 37°C unless otherwise noted. All information on alternate temperature conditions, as well as media conditions for experiments, can be found in the method details section.

Please cite this article in press as: Lobritz et al., Increased energy demand from anabolic-catabolic processes drives β-lactam antibiotic lethality, Cell Chemical Biology (2021), https://doi.org/10.1016/j.chembiol.2021.12.010

METHOD DETAILS

Bacterial strains, media, growth conditions, and time-kill experiments

Experiments were conducted in *E. coli* K12 strain MG1655 (ATCC no. 700926). Rich media experiments were conducted in LB medium unless otherwise specified (Difco). All metabolite measurement experiments were performed in laboratory-made M9 minimal media supplemented with 10 mM glucose as the sole carbon source (M9G). Metabolite supplementation experiments were conducted by adding commercially available pooled nucleobases, pooled amino acids, or both (Teknova) to M9G. Antibiotics were purchased from Sigma. Unless specifically annotated, mecillinam was added at 10 μg/mL, chloramphenicol was added at 50 μg/mL, A22 was added at 10 μg/mL, and glutathione was added at 10 mM. For time-kill experiments, overnight bacterial cultures were grown in the same media type in which the subsequent time-kill experiment was performed to avoid diauxic shifts. For time-kill experiments in LB, cultures were diluted 1:1000 from the overnight culture into 25 mL of LB in 250 mL baffled flasks and grown until an OD_{600} of 0.1 – 0.2, at which time the cultures were then back-diluted to an OD_{600} of ~0.01 in 25 mL of the appropriate test media in 250 mL baffled flasks, and then the indicated antibiotic was added. For time-kill experiments in M9G, cultures were diluted 1:100 from the overnight culture into 25 mL of M9G in 250 mL baffled flasks and grown to an OD_{600} of ~0.01 and then the indicated antibiotic was added. Aliquots were taken at specified time intervals, subjected to serial 10-fold dilution, and spotted onto LB agar without antibiotics to determine quantitative colony-forming units (CFU).

Morphology analysis of mecillinam-treated cells in different media conditions

For morphology analysis of mecillinam-treated *E. coli* MG1655 grown in different media conditions, overnight cultures were diluted into 5 ml of fresh LB or M9G in 14 ml polypropylene tubes and grown for 3 hr to reach an OD_{600} of ~0.15. Cells were then diluted into fresh LB or M9G to an OD_{600} of 0.1 and a sample was taken for imaging. The remaining culture was treated with 10 μg/mL of mecillinam for 3 hr and then imaged. For imaging, immediately after sampling, cells were concentrated by centrifuging at 3500 rpm for 5 min and resuspended in a smaller volume. We placed 2 μL of the resuspended culture on top of a slide and 1.5 mm agarose pad (1.5%) made with the respective growth media followed by a coverslip and then the culture was imaged (Zeiss Axioscope A1).

Measurement of extracellular metabolites

To measure extracellular metabolites, bacteria were diluted to an OD_{600} of 0.05 from an overnight culture grown in M9G and then grown in 25 mL in 250 mL baffled flasks to an OD_{600} of 0.1 for the start of the experiment. At defined time points, aliquots of bacteria were obtained for CFU counts and metabolite quantification. Growth medium was prepared for measurement by centrifugation to remove bacteria in suspension and filtration through a 0.2 μm filter. Samples were stored and batch measured for metabolites in triplicate. Concentrations of extracellular glucose, acetate, formate, and lactate were measured according to the manufacturer's instructions using colorimetric kits (Sigma).

Measurement of extracellular oxygen and acid flux

Bacterial oxygen consumption rate (OCR) and extracellular acidification rate (ECAR) were measured on a Seahorse XFe96 Extracellular Flux Analyzer (Agilent Technologies). Overnight cultures of specified bacterial cultures were diluted 1:100 into fresh M9 media with 10 mM glucose (M9G) and grown to an OD_{600} of approximately 0.3. Cells were diluted to 2x the final optical density and added to the XF Cell Culture Microplates that had been pre-coated with poly-D-lysine as an adherent. The plates were centrifuged at 1400 x g for 10 min in a Heraeus Multifuge x 1R (M-20 rotor), so as to attach cells to generate a monolayer of adhered cells from the suspension. 90 μL of additional fresh, cold M9G media was added to bring up to a final volume of 180 μL prior to antibiotic injection. Cells were warmed rapidly to 37°C, and OCR and ECAR were monitored over time in the flux analyzer and in response to antibiotic perturbations introduced at defined time points.

Measurement of intracellular metabolites

MG1655 was grown overnight in 14 mL tubes in freshly made M9G for 18 hr until the cells reached mid-log phase or OD_{600} of approximately 0.3. Mid-log phase cultures were then back diluted to an OD_{600} of 0.05 in a total of 200 mL in 2L baffled flasks and grown for approximately 90 min in fresh M9 glucose until reaching the goal OD_{600} of 0.1, which was designated as time 0. A fixed volume of 25 mL of culture was collected at each designated time point. Total CFU/mL was determined by limiting dilution CFU assay. Viable cells were concentrated by centrifugation at 5000 x g for 10 min at 4°C. Supernatants were filter sterilized and frozen at −80°C for subsequent extracellular metabolite analysis. Cell pellets were washed in 1 mL ice-cold purified water, re-centrifuged, and metabolites were extracted with 1.6 mL methanol. Metabolites were column purified, methanol was removed by centrifugal vacuum concentration, and dried metabolites were frozen at −80°C. For analysis, samples were re-suspended in ultrapure water and metabolites were quantified on an Agilent capillary electrophoresis-time-of-flight mass spectrometry system (CE-TOFMS, Human Metabolome Technologies, Inc.). Triplicate metabolite profiling samples were processed by Human Metabolome Technologies (HMT) to yield: (1) absolute concentration values for 96 intracellular metabolites, and (2) relative abundance for a larger breadth of intracellular metabolites. In both data sets, missing values were imputed with 2^{-52}, and the values were plotted over time with standard error bars. Metabolite profiling was conducted in two runs consisting of an initial pilot run, followed by two replicates in a second metabolomics run. Relative abundance plots represent the average of the two replicates collected in the second run. Principal component analysis (PCA) was performed on the absolute concentration data in Matlab using *pca*() with the singular value decomposition algorithm.

Please cite this article in press as: Lobritz et al., Increased energy demand from anabolic-catabolic processes drives β-lactam antibiotic lethality, Cell Chemical Biology (2021), https://doi.org/10.1016/j.chembiol.2021.12.010

Hierarchical clustering was also performed in Matlab using *clustergram*() with the correlation distance and average linkage metrics. The absolute concentration data were standardized to a mean of zero and a standard deviation of one prior to PCA and clustering, and analyses were performed in Matlab R2014b (The MathWorks, Inc.). P-values for the absolutely quantified metabolites were calculated using the Student's t-Test in Matlab, and the Benjamini & Hochberg method was used to calculate false discovery rate (FDR).

Live-cell, time-lapse microscopy

Fabrication and assembly of the microfluidic device was performed as described in (Lambert and Kussell, 2015). Cells carrying a low-copy plasmid containing the QUEEN-2m fluorescent reporter under the constitutive control of a strong rpsl promoter (Prpsl ::QUEEN2m, Cam resistance, https://benchling.com/s/Nsq6Kwuz) were grown (37°C) to an OD600 of 0.25, concentrated 1000-fold, and inoculated inside the microfluidic device. The inlet port was connected to a nutrient reservoir containing M9G + 50 μg/mL chloramphenicol and the outlet port was connected to a waste reservoir. The microfluidic device was transferred to a temperature-controlled microscope (Leica) and cells were allowed to grow under M9G conditions for 17.5 hr at 25°C before the nutrient reservoir was replaced by one containing M9G + 10 μg/ml mecillinam + 50 μg/mL chloramphenicol. A fluorescence micrograph at 100x magnification was recorded every 5 min using a sCMOS digital camera (Hamamatsu Flash 4.0) during the 17.5 hr incubation in M9G and the following 21.5 hr of mecillinam exposure. Custom epi-fluorescence custom filter sets and LEDs were used to record fluorescent light at 540 nm emission for 405 nm excitation and 490 nm LED excitation. The distribution of 405ex/490ex ratio for cells within the microfluidic chamber was measured in 25 chambers through single cell detection at each time. To reduce measurement error from background signal and autofluorescence, we selected the half of cells with the greatest total intensity level for analysis, which is similar to the method used in the original QUEEN-2m paper (Yaginuma et al., 2014).

Methionine incorporation assay

For the assay development, cells were grown in methionine-free MOPS EZ Rich (MOPS supplemented with complete amino acids minus methionine, Teknova). Alternatively, cells were grown in M9G alone or with supplementation of amino acid (methionine-free) and/or nucleobase complements. Overnight cultures were diluted 1:1000 into methionine-free media and grown to an OD_{600} of 0.25. Cells were distributed into 96-well plates and exposed to relevant antibiotics for 5 min. Component A (Methionine analog/Click-iT HPG) was added and incubated for 25 min. Cells were fixed and permeabilized after centrifugation, PBS washed, and ultimately re-suspended in 100 μL of 4% paraformaldehyde. After 30 min, cells were washed twice in 3% BSA in PBS and resuspended in 0.5% Triton X-100 for 20 min at room temperature. Click-iT reaction cocktail was prepared according to the manufacturer's protocol (Life Technologies), except that AlexaFluor Azide was added to a final concentration of 20 ug/mL. Cells were PBS washed and then resuspended in 100 μL of Click-iT reaction and incubated for 30 min at room temperature. Cells were washed in Component F and resuspended in PBS. Fluorescence was measured using an LSRFortessa cell analyzer equipped with a High Throughput Sampler (BD Biosciences). At least 10,000 cells were collected for each measurement, and FlowJo (BD) was used for data analysis.

Preparation of samples for mecillinam uptake measurements

E. coli MG1655 was diluted 1:1000 from an overnight culture into 50 mL LB in 250-mL flasks. Cells were grown at 37°C with shaking at 300 rpm to an OD_{600} of 0.1, as measured by reading 300 μL of sample volume in a 96-well flat-bottom plate using a SpectraMax M3 spectrophotometer (Molecular Devices, San Jose, CA). For each sample, cells were back-diluted to an OD_{600} of 0.01 by diluting 10 mL culture with 90 mL LB in 250-mL flasks. The 100 mL cell culture was treated with either mecillinam (final concentration 10 μg/mL) or mecillinam (final concentration 10 μg/mL) and glutathione (final concentration 10 mM). After 2 or 4 hr of incubation, 50 mL of cell culture was aliquoted, centrifuged at 3720 × *g* for 10 min, and washed with 500 μL PBS. Cells were centrifuged again at 1500 × *g* for 10 min, the supernatant was discarded, and 500 μL acetonitrile (Sigma-Aldrich 271004) was added to the cell pellet. Samples were then flash-frozen on dry ice and stored at −80°C. Mecillinam concentrations in these samples were determined using liquid chromatography-mass spectrometry (LC-MS), as detailed below. The remaining 50 mL of cell culture was used for protein concentration determination, as detailed below.

Preparation of samples in culture media for mecillinam concentration measurements

For each sample, mecillinam (final concentration 10 μg/mL) or mecillinam (final concentration 10 μg/mL) and glutathione (final concentration 10 mM), was mixed into 5 ml of LB in 14 ml tubes. These samples were then incubated at 37°C with shaking at 300 rpm. After 0, 2, and 4 hr of incubation, 1 ml samples were taken and frozen immediately at −80°C.

Protein concentration determination

Bacterial proteins were extracted following previous work (Wong et al., 2021). 50 mL of cell culture was aliquoted, centrifuged at 3720 × *g* for 10 min, and washed with 500 μL PBS. Cells were centrifuged again at 1500 × *g* for 10 min, the supernatant was discarded, and 1 mL of lysis buffer, B-PER II (product 78260, Thermo Fisher Scientific, Waltham, MA) containing 100 μg/mL lysozyme (Sigma-Aldrich L6876) and 5 U/mL DNase I (Thermo Fisher 90083), was added to each cell pellet for harvesting. After addition of lysis buffer, all samples were vortexed and incubated at room temperature for 30 min. All samples were then centrifuged at 1500 × *g* for 10 min, and the supernatant was aliquoted from each sample and stored at −80°C until the time of assay.

Please cite this article in press as: Lobritz et al., Increased energy demand from anabolic-catabolic processes drives β-lactam antibiotic lethality, Cell Chemical Biology (2021), https://doi.org/10.1016/j.chembiol.2021.12.010

For protein concentration measurements, we used the Coomassie Plus protein assay reagent (Thermo Fisher 23236) following the manufacturer's instructions. Briefly, each supernatant sample was thawed at room temperature, and 10 μL of sample was pipetted directly into 300 μL of Coomassie Plus reagent in a 96-well plate. The plate was mixed and incubated at room temperature for 10 min, and the absorbance at 595 nm was read using a SpectraMax M3 spectrophotometer. Standard curves were generated from control samples with bovine serum albumin (BSA) concentrations of 2000, 1500, 1000, 750, 500, 250, 125, 25, and 0 μg/mL, where BSA was diluted in the same lysis buffer used to prepare samples. Protein concentration values were inferred by linearly interpolating absorbance values with respect to the standard curves.

Mecillinam concentration measurements with LC-MS

LC-MS experiments were performed at the Harvard Center for Mass Spectrometry. Deuterated ampicillin, ampicillin-d_5 (product 25356, Cayman Chemical Company, Ann Arbor, MI), was used as an internal standard. All solvents used are LC-MS grade.

For cell pellets, 300 μL of acetonitrile and internal standard (ampicillin-d_5 at 0.33 μM) was added to frozen samples. 200 μL of H_2O was added, and samples were left to thaw. Samples were vortexed for 30 s, then incubated in an ultrasound bath for 30 min. Samples were then centrifuged at max speed for 20 min, transferred to new tubes and dried under N_2 flow, and resuspended in 100 μL of acetonitrile (50% in water).

For media samples, 50 μL of each sample was transferred to new tubes. 300 μL of acetonitrile and internal standard was added to each sample. Each sample was vortexed for 30 s and centrifuged at max speed for 20 min. The supernatant was then transferred to new tubes, dried under N_2 flow, and resuspended in 100 μL of acetonitrile (50% in water).

A standard curve was prepared using nine 1/5 dilution series of a 1 mM solution of mecillinam in LB. 50 μL of each standard was prepared similarly to the media samples. The lower limit of quantification was found to be 2.5 nM.

All samples were run on an Agilent 6460 Triple Quad Mass Spectrometer coupled to a 1290 LC. The column used was Phenomenex Kinetex C18, 1.7 μm, 100 Å, 150 × 2.1 mm. The source used was ESI turbojet, with gas temperature 330°C, gas flow 8 L/min, nebulizer 40 psi, sheath gas 375°C at 9L/min, capillary at +2800 V and nozzle at +300 V, and delta EMV of +100. The mobile phases were A: water, 0.1% formic acid and B: acetonitrile, 0.1% formic acid. The following gradient was used: 5 min at 0% B, then to 100% B in 10 min, followed by 5 min at 100% B. The column was then equilibrated at 0% B for 5 min. The flow rate was 0.2 mL/min. Each sample was injected twice continuously, and resulting measurements of mecillinam concentration were averaged.

QUANTIFICATION AND STATISTICAL ANALYSIS

The number of biological replicates and meaning of error bars can be found in the figure legends. Matlab was used for the analysis of the metabolomics data as described in the corresponding method details section. FloJo was used for the analysis of flow cytometry data as described in the corresponding method details section.